Experimental Investigation of UWB Impulse Response and Time Reversal Technique Up to 12 GHz: Omnidirectional and Directional Antennas

Amir Dezfooliyan, *Student Member, IEEE*, and Andrew M. Weiner, *Fellow, IEEE*

***Abstract*—An experimental study of the time reversal (TR) technique is presented in a single-input–single-output configuration over the frequency range of 2–12 GHz. A special emphasis of this work is to investigate and compare impulse response (IR) and TR characteristics for omnidirectional biconical and directional spiral antennas over realistic indoor ultrawideband (UWB) channels in both line-of-sight (LOS) and non-line-of-sight (NLOS) environments. We discuss the effects of channel multipath dispersion and antenna frequency-dependant delay distortions on the received responses in both time and frequency domains. The effectiveness of TR for waveform compression is characterized by computing root mean square delay spread and peak-to-average power ratio. Our study suggests that the effectiveness of time reversal is subject to a tradeoff between competing effects—namely, compensation of spectral phase variation (which leads to compression) and aggravation of spectral amplitude structure (which opposes compression). Although TR is a powerful technique for compensation of phase distortions associated with broadband frequency-independent antennas (as shown in LOS experiments with spiral antennas), it shows only modest performance in compressing time spread associated with multipath delays.**

***Index Terms*—Antenna dispersion, channel propagation measurement, directional antenna, multipath channel, omnidirectional antenna, time reversal (TR), ultrawidebandwidth (UWB).**

I. Introduction

ULTRAWIDEBAND (UWB) [1] is an emerging technology for short-range, high-speed wireless communication that offers several unique advantages over conventional narrowband systems (i.e., fading robustness and high data rate capabilities [2]). Due to the large frequency bandwidth of 3.1–10.6 GHz, temporal resolutions of UWB systems, which are inversely proportional to the bandwidth of the transmitted signals, are extraordinarily fine. This provides the capability to resolve most of the multipath components (MPCs) incident at the receiver. As a result, the received response consists of different components, which have certain delays and attenuations due to the paths they took in their propagation from the transmitter (Tx) to the receiver (Rx).

Manuscript received May 14, 2011; revised December 27, 2011; accepted January 24, 2012. Date of publication April 30, 2012; date of current version July 02, 2012. This work was supported in part by the Naval Postgraduate School under Grant N00244-09-1-0068 under the National Security Science and Engineering Faculty Fellowship Program.

The authors are with the School of Electrical and Computer Engineering, Purdue University, West Lafayette, IN 47907 USA (email: amir@purdue.edu).

Color versions of one or more of the figures in this paper are available online at http://ieeexplore.ieee.org.

Digital Object Identifier 10.1109/TAP.2012.2196927

To capture and process received energies that are dispersed over a large number of MPCs, complex receiver systems (i.e., Rake receivers [3]) are necessary. Time reversal (TR) is a transmission technique that can be used in UWB systems to shift the receiver complexities to the transmitter side. TR is based on the reciprocity of the wave equations and was originally proposed as a solution to compensate inhomogeneous media's distortion [4]. In TR, channel impulse response is flipped in time domain and used as a prematched filter in the transmitter side. The time-reversed waveform is propagated back through the same channel, and multipath components add up coherently at the intended receiver at a particular time after traveling through different paths.

Time-reversal performances have been investigated by several authors for UWB communications [5]–[14]. However, the majority did not implement TR experimentally, and their analyses are based on the TR simulation that is basically the autocorrelation of the impulse response of the channel [5]–[9]. TR performances have been simulated based on IEEE proposed UWB multipath channel model in [5]–[7]. In [8] and [9], TR space-time focusing performance is studied based on simulations by taking autocorrelation and cross correlation of the measured channel impulse responses that give an ideal prediction of TR capabilities when the measured data are noise-free and the estimated channel impulse responses are perfectly accurate.

A few other researchers have studied UWB-TR experimentally by exciting the channel with the reversed version of the measured impulse response [10]–[14]. Guo *et al.* [10] used two omnidirectional antennas 5 m away from each other and blocked the line-of-sight (LOS) path by a bookshelf. Experiments were carried out in the frequency range of 3.5–4.5 GHz, with impulse response measurements performed by using a vector network analyzer (VNA). In [12] and [13], experimental TR is conducted for omnidirectional antennas with approximately 8 m propagation distance. Measured impulse responses are reversed, truncated, and resampled in time to construct appropriate TR waveforms for generating with an arbitrary waveform generator (AWG). Their measurements are limited to the band of 0.7–2.7 GHz. In [14], the same model of AWG has been used to analyze space-time focusing of TR over 6.6 m separation distance for omnidirectional antennas. These experimental literatures either cover a small portion of the UWB or are completely out of this band.

In this work, we measure impulse responses in time domain by using spread spectrum channel sounding. We excited

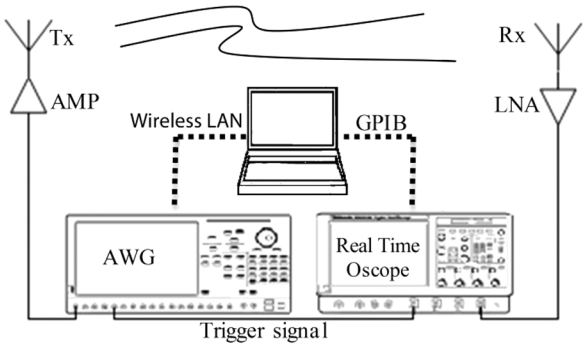

Fig. 1. Block diagram of the measurement system.

channels by chirp signals that cover the frequency range of 2–12 GHz and implemented post-processing method introduced in [15] and [16] to extract the impulse responses from the received waveforms. For each channel measurement, time reversal technique was experimentally applied by generating the time-reversed version of the channel with an AWG. We conducted our measurements over 15 locations in LOS and 15 locations in non-line-of-sight (NLOS) environments. Experimental TR results were compared to TR simulations to show the accuracy of our measurements. A special emphasis of this work is to assess capabilities of TR technique in suppression of multipath dispersions and antenna distortions in LOS and NLOS environments. For this purpose, impulse response (IR) and TR characteristics are studied for spiral directional and biconical omnidirectional antennas, by calculating "root mean square delay spread" and "peak-to-average power ratio." For biconical antennas, channel multipath dispersions are the main reason for the delay spreads, while for spiral antennas, frequency-dependent delays of the antennas significantly modify signals upon radiation and reception. Based on our measurements, time reversal is a powerful technique to compensate antennas distortions. However, it is less effective in compressing UWB channel multipath effects.

The remainder of this paper is organized as follows. Section II provides details of the measurement setup, environment layout, measurement methodology, and TR technique. Section III introduces different parameters to characterize delay spread and temporal compression of IR and TR experiments. Examples of the IR and TR measurements, for both biconical and spiral antennas, are reported in Section IV. Also in this section, the experimental results are analyzed, and TR performance is compared for different antenna types in both LOS and NLOS environments. Finally, in Section V, we conclude.

II. Measurement Configuration

A. Experimental System and Measurement Method

Fig. 1 shows the block diagram of the measurement system. The main components of the transmitter block are an arbitrary waveform generator (Tektronix AWG 7122B), an ultrabroadband amplifier (Picoseconds Pulse Labs 5828A), and the transmitting antenna. The AWG is used in interleaving mode with an effective RF bandwidth (-6 dB) of 9.6 GHz and maximum sampling rate of 24 GS/s. The received signal after amplification

Fig. 2. Environment layout. Tx1 and Rx1 show respectively the positions of the transmitter and the receiver grid for the LOS measurements. Tx2 and Rx2 are the corresponding locations for the NLOS experiments.

is directly connected to a real-time oscilloscope (Digital Serial Analyzer, Tektronix DSA 72004B) with 20 GHz analog bandwidth and maximum real-time sampling rate of 50 GS/s. We have used two different antennas in our experiments: directional Archimedean spiral antennas (NURAD 9C41600, 2–18 GHz), which are strongly dispersive and have circular polarization, and wideband omnidirectional biconical antennas (ELECTROMETRICS EM-6865, 2–18 GHz), which have vertical polarization and uniform radiation pattern in the azimuth plane. More detail about our measurement setup is provided in [15].

Measurements have been carried out in the subbasement of the MSEE building at Purdue University, West Lafayette, IN, for which the floorplan is shown in Fig. 2. Channel propagations and TRs are studied in different locations for omnidirectional and spiral antennas, in LOS and NLOS environments. To observe channel variations, in each scenario the Rx antenna is moved along a track to scan a 1.2×2.4-m^2 area, while the Tx antenna is kept at the same location. The minimum interelement spacing over each grid is 60 cm, which corresponds to 15 total measurement points. The LOS experiments (Tx1–Rx1) were conducted in a large laboratory (room 40 in Fig. 2) that contains metallic desks, cabinets, computers, and scattering objects of different sizes with average propagation distance of 3.5 m. For NLOS measurements (Tx2–Rx2), we placed the transmitter in the laboratory 40 and the Rx in room 39 across from the laboratory. In this case, there are two cement walls and a hallway in the direct path of the Rx-Tx antennas, and the average propagation distance is 14 m. For directional spiral antennas, we aligned the Rx and Tx antennas to aim at each other, while in omnidirectional scenarios, signals are propagated and received in all directions, and alignment is not required.

In this paper, we used an up-chirp signal defined over 0–12 GHz with 85.3 ns time aperture at 24 GS/s frequency rate for probing the channel. To extract impulse responses from the received waveforms, a deconvolution method [15] is implemented. First, we record the sounding waveform without wireless transmission (the AWG output is connected to the

oscilloscope by a RF cable). Then, the received response that is propagated through the channel and antennas is deconvolved from the sounding waveform. The accuracy of this method is studied in [15], which demonstrated that independent measurements (using different sounding waveforms) produced nearly identical results, with correlation coefficients of 0.99 or better even in NLOS environments.

B. Time Reversal Technique

As we mentioned, in an ideal case, the received response from TR can be modeled as the autocorrelation of the impulse response of the system, which is a symmetric waveform. TR simulation can be expressed mathematically, in time and frequency domains, respectively, as:

$$y_{\mathrm{TR}}(t) = h^*_{\mathrm{Sys}}(-t) * h_{\mathrm{Sys}}(t) \tag{1}$$

$$Y_{\mathrm{TR}}(\omega) = H^*_{\mathrm{Sys}}(\omega) \cdot H_{\mathrm{Sys}}(\omega) = |H_{\mathrm{Sys}}(\omega)|^2 \tag{2}$$

where * denotes the convolution operation; $h_{\mathrm{Sys}}(t)$ and $H_{\mathrm{Sys}}(\omega)$ are the measured impulse response of the channel, antennas, and amplifiers; and $y_{\mathrm{TR}}(t)$ and $Y_{\mathrm{TR}}(\omega)$ are the expected responses of TR technique, respectively, in time and frequency domains. In (1), although h_{Sys} and y_{TR} are real, since we are considering them to be baseband signals, we retain the complex conjugate so that (1) is also applicable to the case where h_{Sys} and y_{TR} are envelope functions with an assumed carrier. As we can see in (2), TR compensates the spectral phase of the transfer function, and Y_{TR} is equal to the square magnitude of the H_{Sys}.

In experimental measurements, transmitted signals from AWG and received waveforms by the oscilloscope are modified, respectively, by the impulse response of the AWG $(h_{\mathrm{AWG}}(t))$ and of the oscilloscope $(h_{\mathrm{Oscope}}(t))$. We used the deconvolution method to measure the combined AWG and scope response by dividing the spectral amplitude of the chirp signal recorded at the output of the AWG by the spectral amplitude of the ideal chirp waveform. These undesired effects are compensated in our measurements by programming the AWG with the waveform $x(t)$, which in frequency domain can be expressed as

$$X(\omega) = \frac{H^*_{\mathrm{Sys}}(\omega)}{H_{\mathrm{AWG}}(\omega) H_{\mathrm{Oscope}}(\omega)}. \tag{3}$$

When this waveform is constructed with the AWG, if there is no noise and if our response measurements are perfectly accurate, then the recorded TR waveform by the oscilloscope should be equal to the simulation, $y_{\mathrm{TR}}(t)$, in (1). To assess the accuracy of the experimental TR, we compare it to the simulation result and compute the correlation coefficient between the two datasets for each channel measurement.

III. Channel Characterization Metrics

In order to characterize the delay spread of the measured impulse response and the quality of time reversal, different parameters can be defined. One of the most useful parameters that affects the data transmission rate over the channel is root mean square (RMS) delay spread. The RMS delay can be used as a practical parameter to measure the time dispersion introduced by multipath channels (when Tx and Rx are omnidirectional antennas) and antennas dispersion (when highly dispersive antennas exhibiting frequency-dependent delay behavior are used). This quantity is given by

$$\sigma \equiv \left[\frac{\int_0^\infty d\tau (\tau - \bar{\tau})^2 |s(\tau)|^2}{\int_0^\infty d\tau |s(\tau)|^2} \right]^{1/2} \tag{4}$$

where

$$\bar{\tau} \equiv \frac{\int_0^\infty d\tau \tau |s(\tau)|^2}{\int_0^\infty d\tau |s(\tau)|^2} \tag{5}$$

In (4) and (5), $|s(\tau)|$ is the positive gain of the impulse response of the channel or the received response from TR excitation at delay τ relative to the first detectable signal arriving at $\tau_0 = 0$. In general, channel characteristic metrics strongly depend on the selected noise floor level. This threshold level should be as low as possible to capture all the real energies, but high enough to avoid the noise effects [17]. In our calculations, we define 37 dB threshold level respect to the maximum power and set all components below this level equal to zero. In each measurement, we averaged over a large number of waveforms (3000) in order to bring the noise floor sufficiently below the defined threshold that channel performance parameters can be obtained accurately. In a practical system, this level of accuracy is not required, and one would not perform such averaging.

To evaluate the temporal focusing effectiveness of TR, we calculate and compare σ for IR and TR experiments in different situations. We define a temporal compression parameter C_{rms}

$$C_{\mathrm{rms}} = \frac{\sigma_{\mathrm{IR}} - \sigma_{\mathrm{TR}}}{\sigma_{\mathrm{IR}}} \times 100 \tag{6}$$

where σ_{IR} and σ_{TR} are, respectively, the RMS delay values of the impulse response, and the corresponding received response from the TR experiment. The parameter C_{rms} provides a measure of the TR temporal focusing gain. We expect this ratio to be as high as possible to have a good compression by TR technique. Negative values of C_{rms} show TR increases the RMS delay spread of the channel. In [18]–[20], it is shown the RMS delay spread increases by TR technique in some environments. However, no physical explanation was provided for this phenomenon. In our work, we look at the system transfer functions, $H_{\mathrm{Sys}}(\omega)$, to physically elucidate the cause of TR performance deterioration in some environments.

In another route, to show the time compression quality of TR, we define a parameter ϑ, which is the ratio of the peak to the average power (PAPR) of the waveform presented in decibels

$$\vartheta = 10 \log \left(\frac{\max \left\{ |s(t)|^2 \right\}}{\frac{1}{T} \int_0^T dt |s(t)|^2} \right). \tag{7}$$

This quantity is especially important for receivers in which the decision criterion is based directly on thresholding. When TR results in time focusing and concentration of the power in few taps, we expect ϑ to be larger than the corresponding value for the impulse response measurement. We measure ϑ over a

TABLE I
CHARACTERIZATION METRICS FOR THE OMNIDIRECTIONAL AND SPIRAL RESPONSES PRESENTED IN FIGS. 3, 4, 6, AND 7. THE LOS IR AND TR VALUES ARE BASED ON THE RESPONSES SHOWN RESPECTIVELY IN FIGS. 3 AND 4. THE NLOS IR AND TR PARAMETERS ARE ALSO CALCULATED FOR THE RESPONSES IN FIGS. 6 AND 7

	Antenna	Experiment	RMS delay σ (ns)	PAPR ϑ (dB)	Temporal Compression Gain C_{rms} (%)	PAPR Gain G_ϑ (dB)
LOS	Omnidirectional	Impulse response	13.98	30.3	-1.3%	0.0dB
		Time Reversal	14.16	30.3		
	Spiral	Impulse response	4.67	23	50%	11.23dB
		Time Reversal	2.35	34.23		
NLOS	Omnidirectional	Impulse response	21	21.95	7.2%	6.17dB
		Time Reversal	19.5	28.12		
	Spiral	Impulse response	9.5	23.38	25.2%	7.83dB
		Time Reversal	7.1	31.21		

200-ns time window for all experiments and present values in decibel. To evaluate PAPR gain provided by TR, a parameter G_ϑ is defined (in decibels) as

$$G_\vartheta = \vartheta_{\mathrm{TR}} - \vartheta_{\mathrm{IR}} \tag{8}$$

where ϑ_{IR} and ϑ_{TR} are, respectively, the PAPR values of the impulse response and the corresponding received response from the TR experiment. The parameter G_ϑ provides insight about the PAPR gain achieved by implementing TR technique.

IV. IMPULSE RESPONSE AND TIME REVERSAL EVALUATION

In this section, we investigate IRs and TR performances for spiral and omnidirectional antennas. We have chosen these two antennas because they are affected by different important physical interactions. With the omnidirectional antennas, the transmitted signals from the Tx can propagate in all directions and reach the Rx via different paths and interactions (e.g., reflection, diffraction, or scattering). The received responses in these experiments consist of different components that have certain delays and attenuations. On the other hand, the spiral antennas are directional and strongly dispersive (caused by the frequency-dependant delay characteristic of these antennas). Here, distortions due to the antennas themselves affect the received responses, and the number of multipath components received is reduced compared to the omnidirectional case. In particular, in LOS experiments the measured impulse response for spiral antennas is dominated by the antenna's dispersion (frequency-dependent delay). This results in significantly different TR performance compared to other scenarios in which multipath propagation is important.

Impulse responses of spiral and omnidirectional antennas have been studied separately in a number of papers in the literature, but to our knowledge, there is no comprehensive work to investigate and compare directional and omnidirectional responses and TR performances together. Impulse responses of spiral antennas in different bandwidths for LOS environment have been studied in [22] and [23]. In [23], they extracted nonuniform phase characteristics of the antennas and excited the Tx antenna with waveforms designed to compensate the phase response. These references used a photonics-based arbitrary electromagnetic pulse shaper to generate the exciting waveforms. For omnidirectional antennas, Molisch *et al.* [24] presented a comprehensive statistical model based on measurements and simulations for different environments in the frequency range of 3–10 GHz. In [17], indoor UWB channels were characterized in the time domain by using a 100-ps Gaussian-like waveform with approximately 7 V amplitude peak; impulse responses were studied for directional TEM horn and omnidirectional biconical antennas in both LOS and NLOS environments. The main focus of [17] was to study the statistical behavior of the impulse response for directional and omnidirectional antennas; investigation of TR characteristics for these links was not considered.

In Sections IV-A and IV-B, we compare IRs and TR qualities of spiral and omnidirectional antennas in LOS and NLOS environments. In each section, we first study a specific (but typical) impulse response for the omnidirectional antennas and compare in detail to the measured response of the spiral antennas placed at the same locations. Time reversal is then implemented for these scenarios, and performances are fully investigated in Table I. The typical presented LOS and NLOS experiments have propagation distances of 3.5 and 14 m, respectively. We used 10-dB gain amplifiers on the Tx side and excited the antenna with the AWG using the maximum available peak-to-peak voltage of 0.5 V. In the Rx side, we have 41- and 51-dB amplifier gains, respectively, for LOS and NLOS measurements. Finally at the end of each section, we repeat our experiments with the receiving antenna moved over a rectangular grid and report the average and standard deviation of IR and TR performance metrics in Table II. Finally, Table III summarizes the key results of this section.

A. Line-of-Sight Environment

Fig. 3 compares the impulse responses of LOS omnidirectional and spiral experiments over a 100-ns time window. In the small subfigures, we zoom in on the first 10 ns of the power delay profile (PDP) of the responses to better show their characteristics. The PDPs are obtained by taking the magnitude squared of the impulse responses. We can see there are two main components in the impulse response of omnidirectional antennas. The first, dominant received signal comes from the direct LOS path between the antennas. The sharp LOS signal proves the omnidirectional antennas have low dispersion (low frequency-dependent delay). The second multipath component, which is $\sim$6 dB less than the direct path with a reversed amplitude sign, comes from a large metal rack on the left side of the Rx antenna. Spiral antennas are directional and strongly dispersive, so the measured impulse response is dominated by the frequency-dependent delay of the antennas rather than

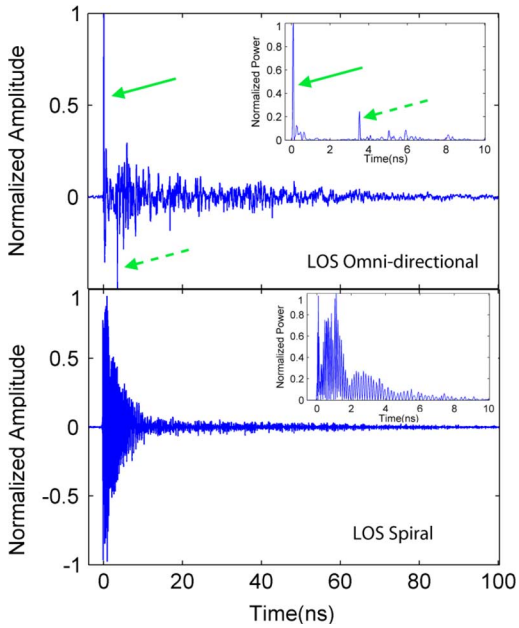

Fig. 3. Impulse responses of LOS omnidirectional and spiral antennas over 100-ns time windows. Power delay profiles of these experiments are shown over 10-ns time windows. Arrows indicate two main components in the omnidirectional responses.

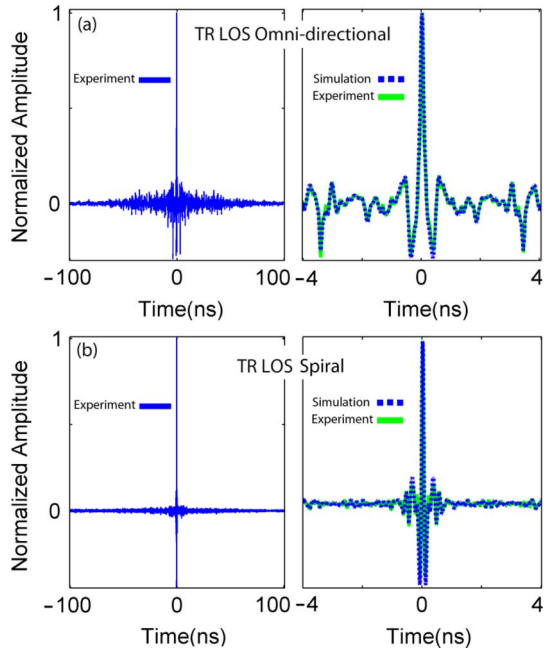

Fig. 4. (a), (b) Experimental time reversal for LOS omnidirectional and spiral antennas over 200-ns time window. On the right side, we compare experimental and simulated TRs over smaller time windows to show the accuracy of our measurements.

multipath effects. Our measured impulse response extends mainly over ∼8 ns and shows a strong down-chirp characteristic that is similar to what was reported in [22]. To investigate the severity of the channel dispersion and antenna distortion for omnidirectional and spiral antennas, respectively, we look at the parameters σ and ϑ for the LOS impulse responses in Table I. Comparing RMS delay values show the omnidirectional response is dispersed over a longer time period compared to the spiral impulse response. Powers for omnidirectional and spiral antennas are received in two different patterns. In the absence of good reflectors in the environment, power delay profiles of omnidirectional antennas can be considered as a single exponential decay with a strong LOS component [21]. Effects of the first dominant component on the parameters σ and ϑ can be understood by calculating them for the impulse response excluding the first LOS signal. These parameters become $\sigma = 16.3$ ns and $\vartheta = 24.7$ dB after removing the first 300 ps of the omnidirectional impulse response. Comparing these values to Table I (which is based on the whole IR), we can see that without the first 300 ps, the PAPR reduces ∼5.6 dB and the rms increases ∼14.2%. This shows the important effect of the LOS component. However, we have a different situation for the spiral impulse response. Spiral antennas are highly directional, and the impulse response has much fewer multipath components compared to the omnidirectional case. In this case, the response is dominated by the LOS component distorted according to the frequency-dependent delay of the antennas. If we calculate the aforementioned parameters for the spiral impulse response excluding the first 300 ps, they become $\sigma = 4.9$ ns and $\vartheta = 23.6$ dB, which are comparable to the original parameters presented in Table I.

Experimental TR results for impulse responses shown in Fig. 3 are presented on the left side of Fig. 4(a) and (b) over 200-ns time windows. The simulations and experiments of TRs are also compared over smaller time windows to better show the accuracy of our measurements. We can see these curves match peak for peak, and there is at most a few percent difference between simulations and experiments. The correlation coefficients between simulations and experimental TR traces are, respectively, 0.991 and 0.966 for omnidirectional and spiral scenarios, which shows excellent agreement.

To investigate the achieved gains by implementing TR, we compare the parameters σ, ϑ, $C_{\rm rms}$, and G_ϑ for the LOS TRs in Table I. For the spiral experiment, the PAPR value is increased 11.23 dB and the RMS delay spread is significantly shortened (∼3 dB) after implementing TR technique. The response is symmetric, and the energy is mainly concentrated around the symmetric point, which means, in practical communication systems, a simpler receiver structure would be sufficient to capture a significant amount of the received power.

For the omnidirectional antennas, zero PAPR gain (G_ϑ) shows TR does not improve the ϑ value. Presence of the dominant strong LOS component in the omnidirectional impulse response is the main reason for this poor TR performance. As we previously showed, removing the main LOS signal reduces ϑ from ∼30.3 to ∼24.7 dB, which shows the important effect of the LOS component on the PAPR value. In general, TR shows better PAPR gains when the strong taps of the impulse response are distributed over time. In the spiral case, there is no single strong dominant component, and TR gives a good PAPR gain value.

The negative temporal focusing $(C_{\rm rms} = -1.3\%)$ implies that TR cannot decrease the RMS delay spread of the channel, which is consistent with the results predicted by simulations in [20]. To explain the poor LOS TR performance of omnidirectional compared to the spiral antennas, we look at the frequency

TABLE II
AVERAGE (AVG) AND STANDARD DEVIATION (STD) VALUES FOR OMNIDIRECTIONAL AND SPIRAL EXPERIMENTS OVER 15 DIFFERENT LOS LOCATIONS AND 15 DIFFERENT NLOS LOCATIONS. IN THE TEXT, WE REFER TO IMPULSE RESPONSE METRICS BY "IR-METRICS NAME" (E.G., SPIRAL IR-PAPR MEANS THE AVERAGE PAPR VALUE FOR SPIRAL IMPULSE RESPONSE MEASUREMENTS). TR NOTATION IS ALSO USED FOR TIME REVERSAL METRICS

			RMS delay σ (ns)		PAPR ϑ (dB)		Temporal Compression Gain C_{rms} (%)		PAPR Gain G_{ϑ} (dB)	
			Avg	Std	Avg	Std	Avg	Std	Avg	Std
LOS	Omni-directional	IR	14.3	1.1	29.8	1.5	-7.8	16.9	0.8	1.6
		TR	15.5	3.0	30.6	0.5				
	Spiral	IR	5.56	0.68	23.0	0.25	44.3	10.4	11.0	0.35
		TR	3.13	0.87	34.0	0.23				
NLOS	Omni-directional	IR	19.7	2.01	21.8	1.77	16.4	6.9	5.1	1.7
		TR	16.4	1.4	26.9	0.6				
	Spiral	IR	9.2	1.97	22.8	1.45	16.6	10.4	7.5	1.69
		TR	7.7	2.04	30.3	0.76				

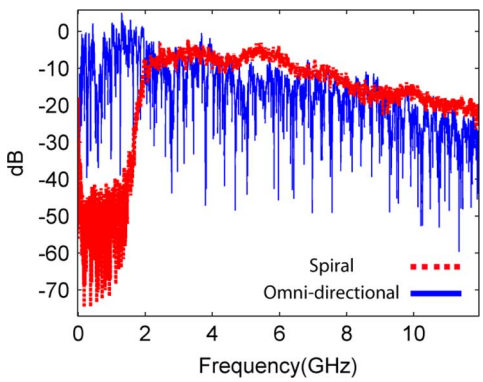

Fig. 5. Frequency responses of the omnidirectional and spiral LOS links computed from the impulse responses shown in Fig. 3. Multipath effects make the omnidirectional spectrum frequency selective, while for spiral antennas, the transfer function is dominated by the antennas' frequency response.

responses of these experiments in Fig. 5. These frequency responses are calculated by taking fast Fourier transform (FFT) of the measured impulse responses shown in Fig. 3. For omnidirectional antennas, the spectrum is significantly frequency selective, which is the direct consequence of the channel multipath effects. Transmitted signals reach the Rx via different paths and experience certain delays and attenuations. The different delay components interfere in the frequency domain, yielding a frequency selective spectrum with many sharp fades. On the other hand, in LOS the transfer function of the directional spiral antennas is dominated by the frequency responses of the antennas. Multipath effects are limited in the directional antennas, and there are no such sharp fades in the spectrum. This result is exactly consistent with the shape of the power spectra measured in [15] by using an RF spectrum analyzer.

As we mentioned in (1) and (2), TR has two principal effects on the frequency domain representation of the received signal: 1) compensating the spectral phase; and 2) squaring the spectral magnitude. The first effect results in concentration of power at the center of the received response and reduces the RMS delay spread of the channel. The second effect shapes the power spectrum, increasing roll-off in the spectrum (e.g., at high frequencies) and accentuating sharp spectral variations (peaks, fades, etc.). Both aspects of the second spectral shaping effect correspond to the aggravation of the overall system amplitude distortion and result in time broadening. Based on whether the phase compensation effect or the spectral shaping effect is stronger, the RMS delay spread of the channel can be either increased or decreased by the TR technique. The amplitude response of the LOS spiral antennas is approximately smooth; phase compensation is the dominant effect, which, overall, reduces RMS delay spread. However, for the LOS omnidirectional antennas, presence of sharp fades in the transfer function makes the broadening effect of the spectral shaping more important. On the other hand, the spectral phase of the received response is dominated by the phase of the LOS component [26], which is essentially subject to no spectral phase variation. Due to this dominant undistorted LOS component, the spectral phase compensation effect provides less compression. As a result of these two phenomena, TR does not give an effective compression performance in the omnidirectional LOS scenario.

As explained earlier, we repeated LOS impulse response and TR measurements over a rectangular grid to observe more channel realizations. In Table II, we summarize average and standard deviation values of the performance metrics for these measurements under the LOS section. In general, standard deviations of spiral links, due to the limited channel multipath effects, are smaller compared to omnidirectional antennas. We investigate effectiveness of TR technique in each scenario by measuring temporal compression and PAPR gains. As we can see, trends of average values are consistent with the physical discussions provided for the typical responses in Fig. 3. Although more measurements are required to derive a statistical model for the gain (e.g., the probability of the negative compression gain in omnidirectional LOS experiments), we can already conclude that TR does not effectively compensate channel multipath dispersion in the LOS regime.

B. Non-Line-of-Sight Environment

In this section, we investigate impulse responses and TRs of omnidirectional and spiral antennas in NLOS environments. Fig. 6 shows the impulse responses of NLOS omnidirectional and spiral experiments over a 200-ns time window. The power delay profiles over the first 10 ns are also presented in two subfigures. For omnidirectional antennas, multipath components

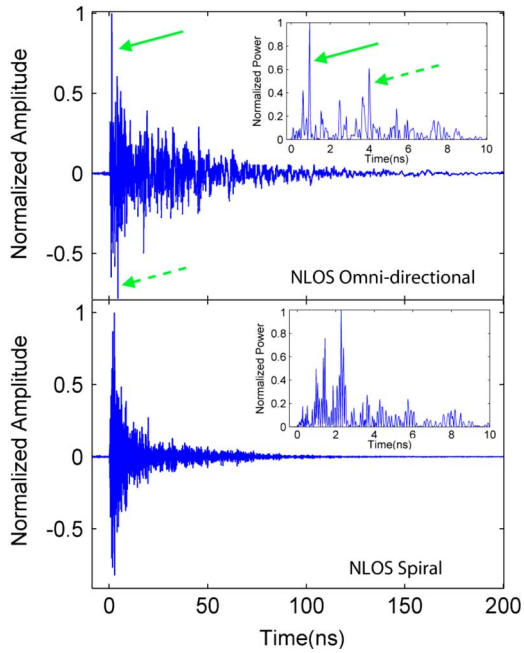

Fig. 6. Impulse responses of NLOS omnidirectional and spiral antennas over a 200-ns time window. Power delay profiles of the omnidirectional and spiral experiments are shown over 10-ns time windows in the small subfigures. The continuous and dashed arrows, respectively, show the first and second strongest components in the NLOS response.

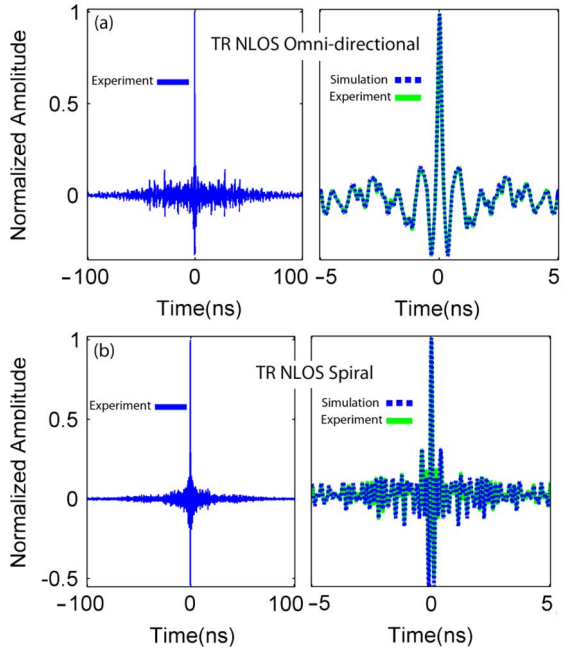

Fig. 7. (a), (b) Experimental time reversal traces for NLOS omnidirectional and spiral antennas over 200 ns. On the right side, we compare experimental and simulated TRs over a smaller time window to show the accuracy of our measurements even in NLOS environments.

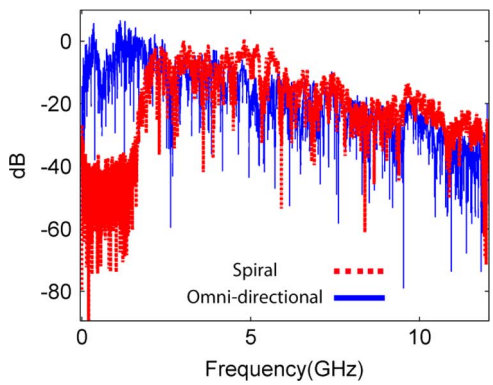

Fig. 8. Frequency responses of the omnidirectional and spiral NLOS links of the impulse responses shown in Fig. 6. Both spectra have a faster decreasing slope [compared to the LOS case (Fig. 5)] due to the longer propagation distance and presence of cement walls in the propagation path. Multipath effects make these spectra frequency selective.

are distributed over time; unlike the LOS case, no strong dominant component exists in the channel response. The second strongest component in this case is just 2.2 dB less than the main one, while for the LOS experiment, this value was in the order of ∼6 dB. Comparison to the omnidirectional impulse response parameters in Table I clarifies the basic differences between the LOS and NLOS responses. The IR-RMS delay of the NLOS channel ($\sigma = 21.0$ ns) is ∼50% larger than the RMS delay of the LOS scenario ($\sigma = 13.98$ ns). The transmitted signals in NLOS environments experience more interactions (reflections, diffractions, etc.) in their paths to the receiver, and therefore more multipath components incident at the Rx. The signal must pass through at least two cement walls to reach the Rx antenna, which increases the high frequency attenuation of the received response [25]. Due to the absence of the strong LOS component, the PAPR value ($\vartheta = 21.95$ dB) is ∼8.3 dB less than the corresponding value for the LOS case.

For spiral antennas, the IR-RMS delay in the NLOS case is approximately two times the spiral LOS situation. Therefore, with the increased antenna separation and the NLOS configuration, multipath effects now contribute more strongly to the delay spread than does antenna frequency-dependent delay. As mentioned earlier, the two cement walls in the path of the antennas also introduce high frequency attenuation. Comparing the NLOS spiral antenna IR-RMS delay to that of the omnidirectional antenna shows multipath effects are still reduced for directional antennas. For LOS spiral experiments, we did not have any dominant component that affects the PAPR value dramatically, so this value for the NLOS case is comparable to the LOS scenario.

TR technique is implemented for these impulse responses, and results are presented in Fig. 7(a) and (b). Simulations and experiments of TRs are compared over 10-ns time windows to better show the accuracy of our measurements. The full width at half-maximum (FWHM) of the TR spiral antenna is 70 ps, while for omnidirectional antennas it is 160 ps. As we show in Fig. 8, the impulse response associated with the spiral antennas has stronger high-frequency content compared to the omnidirectional response (e.g., there is ∼3 dB difference around 10 GHz). For TR experiments, this difference is two times larger in a decibel scale [(2)], which explains the FWHM differences of spiral and biconical antennas. The correlation coefficients between simulations and experiments are 0.9969 and 0.982 for these measurements.

The achieved gains by implementing the TR technique can be analyzed by considering the NLOS C_{rms} and G_{ϑ} parameters in Table I. For omnidirectional antennas, TR performance is

TABLE III
SUMMARY OF AVERAGE PAPR AND TEMPORAL COMPRESSION GAINS PRESENTED IN TABLE II FOR DIFFERENT ENVIRONMENTS AND ANTENNAS. IN THIS TABLE, SYMBOLS "Y" AND "N" REPRESENT PRESENCE AND ABSENCE OF AN IMPULSE RESPONSE CHARACTERISTIC, RESPECTIVELY

		Impulse Response characteristics		TR Performance Parameters	
Environment	Antenna Type	Strong dominant component in IR	Sharp fades in the spectrum	Temporal compression Gain C_{rms} (%)	PAPR Gain G_ϑ (dB)
LOS	Omni-directional	Y	Y	-7.8%	0.8dB
LOS	Spiral	N	N	44.3%	11dB
NLOS	Omni-directional	N	Y	16.4%	5.1dB
NLOS	Spiral	N	Y	16.6%	7.5dB

improved compared to the LOS scenario. Absence of an undistorted LOS component is the main reason for this improvement. However, although TR provides considerable PAPR gain, it still gives only several percent time compression. Again, this can be explained by considering the frequency response of the channel. The omnidirectional received spectrum (Fig. 8) looks like the LOS one, but with a faster decreasing slope. Spectral shaping effect of TR again opposes compression, but due to the absence of the undistorted LOS component (would strongly affect the spectral phase), the phase compensation aspect of TR results in better focusing compared to the LOS omnidirectional scenario, and TR overall provides modest temporal compression.

For the spiral experiment, both gain parameters ($C_{\rm rms}$ and G_ϑ) are worse than the LOS scenario. To understand the reason, we compare the frequency response of the NLOS experiment in Fig. 8 to the corresponding LOS spectrum (Fig. 5). We can see there are several sharp fades in the NLOS frequency response in addition to a faster decreasing slope compared to the LOS spectrum. As mentioned earlier, in spiral NLOS experiments, multipath interactions and the frequency response of obstacles between the antennas (like walls, doors, etc.) become as important as the response of the antennas themselves and lead to interference effects in the frequency response function. The resulting fades in the power spectrum and its faster descending slope are the main reasons for deterioration in TR performance compared to that observed for spiral antennas in an LOS configuration.

To observe more NLOS channel statistics, we moved the receiver over a rectangular grid, while the Tx is fixed during all experiments. Results of these experiments are presented in Table II under the NLOS section. In contrast to the LOS scenario, standard deviations of the metrics for spiral antennas are comparable to the corresponding omnidirectional values (caused by the presence of multipath effects in both NLOS links). The compression and PAPR gains for NLOS omnidirectional antennas shows higher gains can be achieved compared to the LOS experiments, but still temporal compression gain is not significant. In general, implementing TR technique on single-input–single-output (SISO) channels with omnidirectional antennas does not considerably reduce RMS delay spread [20].

To conclude this section, average values of compression gains and PAPR gains for experiments presented in Table II are summarized in Table III. Based on our discussions, there are two important factors that significantly affect TR performance: 1) presence of a strong dominant component in the impulse response (usually an undistorted LOS component); 2) presence of sharp fades in the transfer function of the channel and antennas. We can get the best performance in the LOS spiral antennas in the absence of these two effects, while the worst TR performance is for LOS omnidirectional scenarios, where two effects exist concurrently. For NLOS experiments, presence of sharp fades is the only degrading factor, and an intermediate TR performance can be achieved for both antennas.

V. CONCLUSION

In this paper, we investigated impulse response and TR characteristics of omnidirectional and spiral antennas in LOS and NLOS environments, over the frequency range up to 12 GHz. As we expected, impulse responses of NLOS environments exhibit greater multipath effects, hence more time dispersion, compared to the corresponding LOS experiments. These channel dispersions are particularly significant in omnidirectional antennas that transmit and receive signals in all directions. Time reversal technique was applied to all channels measured, and excellent accuracy of our experiments is proved by comparing the results to TR simulations. "RMS delay spread" and "peak-to-average-power ratio" are calculated as two basic parameters for impulse response and TR performance evaluations. In our experiments, time reversal shows most impressive compression results, as characterized through reduced RMS delay spread and increased peak-to-average-power ratio, for spiral antennas in an LOS configuration, for which effects associated with spectral phase variation dominate. Compression is negligible for omnidirectional antennas in an LOS configuration, for which interference structure in the power spectrum dominates. The compression performance of time reversal is modest for the NLOS configuration studied and is similar for both antenna types; in these cases, both spectral phase variations and variations in the power spectra are important. Thus, the effectiveness of time reversal in SISO experiments is subject to a tradeoff between competing effects—namely, compensation of spectral phase variation (which leads to compression) and aggravation of spectral amplitude structure (which opposes compression).

ACKNOWLEDGMENT

The authors would like to thank Senior Research Scientist Dr. D. E. Leaird for his helpful technical assistance on this work. Any opinion, findings, and conclusions or recommendations expressed in this publication are those of the authors and do not necessarily reflect the views of the sponsors.

REFERENCES

[1] A. F. Molisch, "Ultra-wide-band propagation channels," *Proc. IEEE*, vol. 97, no. 2, pp. 353–371, Feb. 2009.

[2] L. Yang and G. B. Giannakis, "Ultra-wideband communications: An idea whose time has come," *IEEE Signal Process. Mag.*, vol. 21, no. 6, pp. 26–54, Nov. 2004.

[3] Y. Ishiyama and T. Ohtsuki, "Performance comparison of UWB-IR using Rake receivers in UWB channel models," in *Proc. Joint UWBST IWUWBS*, May 2004, pp. 226–230.

[4] M. Fink, C. Prada, F. Wu, and D. Cassereau, "Self focusing in inhomogeneous media with time reversal acoustic mirrors," in *Proc. IEEE Ultrasonics Symp.*, Montreal, Canada, 1989, vol. 1, pp. 681–686.

[5] K. Popovski, B. J. Wysocki, and T. A. Wysocki, "Modelling and comparative performance analysis of a time reversed UWB system," *EURASIP J. Wireless Commun. Netw.*, vol. 2007, 2007.

[6] X. Liu, B.-Z. Wang, S. Xiao, and J. Deng, "Performance of impulse radio UWB communications based on time reversal technique," *Prog. Electromagn. Res.*, vol. PIER 79, pp. 401–413, 2008.

[7] K. Witrisal and M. Pausini, "Statistical analysis of UWB channel correlation functions," *IEEE Trans. Veh. Technol.*, vol. 57, no. 3, pp. 1359–1373, May 2008.

[8] E. Akogun, R. C. Qiu, and N. Guo, "Demonstrating time reversal in ultra-wideband communications using time domain measurements," in *Proc. 51st Int. Instrum. Symp.*, Knoxville, TN, May 2005.

[9] C. Oestges, J. Hansen, S. Emami, A. Kim, G. Papanicolaou, and A. Paulraj, "Time reversal techniques for broadband wireless communication systems," in *Proc. Eur. Microw. Conf. (Workshop)*, Amsterdam, The Netherlands, Oct. 2004, pp. 49–66.

[10] N. Guo, J. Q. Zhang, P. Zhang, Z. Hu, Y. Song, and R. C. Qiu, "UWB real-time testbed with waveform-based precoding," in *Proc. IEEE MILCOM*, 2008, pp. 1–7.

[11] N. Guo, B. M. Sadler, and R. C. Qiu, "Reduced-complexity UWB time reversal techniques and experimental results," *IEEE Trans. Wireless Commun.*, vol. 6, no. 12, pp. 4221–4226, Dec. 2007.

[12] A. Khaleghi, G. E. Zein, and I. H. Naqvi, "Demonstration of time-reversal in indoor ultra-wideband communication: Time domain measurement," in *Proc. ISWCS*, Trondheim, Norway, 2007, pp. 465–468.

[13] I. H. Naqvi, G. El Zein, G. Lerosey, J. de Rosny, P. Besnier, A. Tourin, and M. Fink, "Experimental validation of time reversal ultra-wideband communication system for high data rates," *Microw. Antennas Propag.*, vol. 4, no. 5, pp. 643–650, 2010.

[14] D. Abbasi-Moghadam and V. T. Vakili, "Characterization of indoor time reversal UWB communication systems: Spatial, temporal and frequency properties," *Int. J. Commun. Syst.* vol. 24, pp. 277–294, Mar. 2011.

[15] A. Dezfooliyan and A. M. Weiner, "Time domain propagation measurements of UWB systems using spread spectrum channel sounding," *IEEE Trans. Antennas Propag.*, 2011, submitted for publication.

[16] A. Dezfooliyan and A. M. Weiner, "UWB propagation measurement using spread spectrum channel sounding," in *Proc. IEEE Int. Symp. Antennas Propag.*, Spokane, WA, 2011, pp. 2805–2808.

[17] A. Muqaibel, A. Safaai-Jazi, A. Attiya, B. Woerner, and S. Riad, "Pathloss and time dispersion parameters for indoor UWB propagation," *IEEE Trans. Wireless Commun.*, vol. 5, no. 3, pp. 550–559, Mar. 2006.

[18] P. Kyritsi and G. Papanicolaou, "One-bit time reversal for WLAN applications," in *Proc. IEEE PIMRC*, 2005, vol. 1, pp. 532–536.

[19] F. Monsef, A. Cozza, and L. Abboud, "Effectiveness of time-reversal technique for UWB wireless communications in standard indoor environments," in *ICECom Conf. Proc.*, 2010, pp. 1–4.

[20] C. Zhou, N. Guo, and R. C. Qiu, "Experimental results on multiple-input single-output (MISO) time reversal for UWB systems in an office environment," in *Proc. IEEE MILCOM*, Washington, DC, Oct. 2006, pp. 1–6.

[21] D. Cassioli, M. Z. Win, and A. F. Molisch, "The ultra-wide bandwidth indoor channel—From statistical model to simulations," *IEEE J. Sel. Areas Commun.*, vol. 20, no. 6, pp. 1247–1257, Aug. 2002.

[22] J. D. McKinney, D. Peroulis, and A. M. Weiner, "Time-domain measurement of the frequency-dependent delay of broadband antennas," *IEEE Trans. Antennas Propag.*, vol. 56, no. 1, pp. 39–47, Jan. 2008.

[23] J. D. McKinney, D. Peroulis, and A. M. Weiner, "Dispersion limitations of ultra-wideband wireless links and their compensation via photonically-enabled arbitrary waveform generation," *IEEE Trans. Microw. Theory Tech.*, vol. 56, no. 3, pp. 710–718, Mar. 2008.

[24] A. F. Molisch, D. Cassioli, C.-C. Chong, S. Emami, A. Fort, B. Kannan, J. Karedal, J. Kunisch, H. G. Schantz, K. Siwiak, and M. Z. Win, "A comprehensive standardized model for ultrawideband propagation channels," *IEEE Trans. Antennas Propag.*, vol. 54, no. 11, pp. 3151–3166, Nov. 2006.

[25] G. Tesserault, N. Malhouroux, and P. Pajusco, "Determination of material characteristics for optimizing WLAN radio," in *Proc. IEEE Eur. Conf. Wireless Technol.*, 2007, pp. 225–228.

[26] A. Goldsmith, *Wireless Communications*. Cambridge, U.K.: Cambridge Univ. Press, 2005, pp. 71–77.

Amir Dezfooliyan (S'11) received the B.Sc. degree in electrical engineering from Sharif University of Technology, Tehran, Iran, in 2009, and is currently pursuing the Ph.D. degree in electrical engineering at Purdue University, West Lafayette, IN.

Since 2009, he has been a Graduate Research Assistant with the Ultrafast Optics and Optical Fiber Communications Laboratory, Purdue University. His current research interests are wireless propagation, UWB communications, ultrafast optics, and optical pulse shaping.

Andrew M. Weiner (S'84–M'84–SM'91–F'95) received the D.Sc. degree in electrical engineering from the Massachusetts Institute of Technology, Cambridge, in 1984.

Upon graduation he joined Bellcore, Red Bank, NJ, first as a Member of Technical Staff and later as Manager of Ultrafast Optics and Optical Signal Processing Research. He moved to Purdue University, West Lafayette, IN, in 1992 and is currently the Scifres Family Distinguished Professor of Electrical and Computer Engineering. He is author of the textbook *Ultrafast Optics* (Wiley, 2009), has published six book chapters and more than 250 journal articles, and is holder of over 10 US patents. His research focuses on ultrafast optics signal processing and applications to high-speed optical communications and ultrawideband wireless.

Prof. Weiner is a Fellow of the Optical Society of America and is a member of the US National Academy of Engineering. In 2009, he was named a US Department of Defense National Security Science and Engineering Faculty Fellow. He has served as Co-Chair of the Conference on Lasers and Electro-optics and the International Conference on Ultrafast Phenomena, as Secretary/Treasurer of the IEEE Lasers and Electro-optics Society (LEOS), as a Vice-President of the International Commission on Optics (ICO), and as Chair of the National Academy of Engineering US Frontiers of Engineering Meeting. He has won numerous awards for his research, including the Hertz Foundation Doctoral Thesis Prize in 1984, the Adolph Lomb Medal of the Optical Society of America in 1990, the Curtis McGraw Research Award of the American Society of Engineering Education in 1997, the International Commission on Optics Prize in 1997, the Alexander von Humboldt Foundation Research Award for Senior U.S. Scientists in 2000, and the IEEE Photonics Society Quantum Electronics Award in 2011. He is joint recipient, with J. P. Heritage, of the IEEE LEOS William Streifer Scientific Achievement Award in 1999 and the OSA R.W. Wood Prize in 2008 and has been recognized by Purdue University with the inaugural Research Excellence Award from the Schools of Engineering in 2003 and with the Provost's Outstanding Graduate Student Mentor Award in 2008.